Nanoscale

Accepted Manuscript

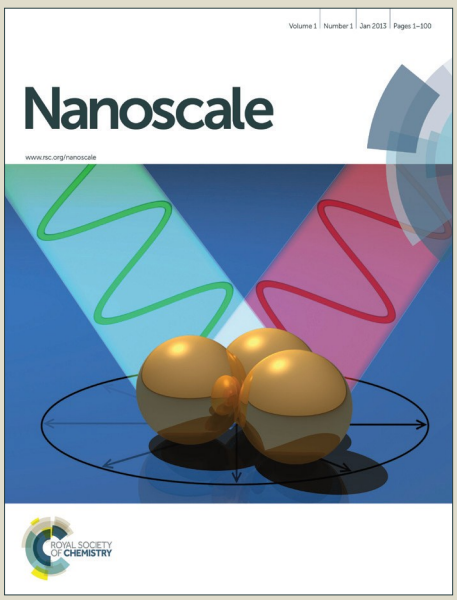

ROYAL SOCIETY OF CHEMISTRY

www.rsc.org/nanoscale

Nanoscale

ARTICLE

CNTs Threaded (001) Exposed TiO_2 with High Activity in Photocatalytic NO Oxidation

Received 00th January 20xx,
Accepted 00th January 20xx

DOI: 10.1039/x0xx00000x

www.rsc.org/

Shuning Xiao,[ab] Wei Zhu,[a] Peijue Liu,[a] Fanfan Liu,[a] Wenrui Dai,[a] Dieqing Zhang,*[,a] Wei Chen,*[, b] and Hexing Li*[, a]

A microwave-ionothermal strategy was developed for *in situ* synthesis of CNTs threaded TiO_2 single crystal with tunable percentage of exposed (001) active facets. The CNTs were used as microwave antennas to create local "super hot" dots to induce Ti^{3+} adsorption and hydrolysis, thereby leading to a well assembly of (001) facets exposed single crystalline TiO_2 threaded by the CNTs with the presence of Hmim[BF_4] ionic liquid. Due to the high percentage of the active (001) facets of single crystal TiO_2 and the direct electron transfer property of the CNTs, the as-prepared CNTs-TiO_2 composite showed a photocatalytic NO removal ratio up to 76.8 % under UV irradiation. In addition, with self-doped Ti^{3+}, the CNTs-TiO_2 composite also exhibited an enhanced activity under irradiation with either solar lights or visible lights, showing good potential in practical applications for environmental remediation.

Introduction

Photocatalysis has been widely studied due to their potential in photosynthesis, environmental cleaning, H_2 production, and photoelectric devices.[1-3] Recently, with the increasing concerns for the air pollution, photocatalytic NO oxidation has received increasing attention in cleaning sweep gas released from vehicles and power plants etc.[4-7] One of the key challenges in photocatalysis is the unfavorable electron-hole separation rate, which is usually much slower than its consumption in chemical reactions.[8,9] To significantly reduce the electron-hole recombination, the photocatalyst should be able to facilitate fast electron transfer and ensure quick consume of photo-induced charges to enhance the oxidation reactions.

TiO_2 has been most frequently employed as a photocatalyst due to its low cost, non-toxicity, high activity and high stability.[10-12] To date, various single-crystalline anatase TiO_2 photocatalysts have been designed for the fundamental studies and practical applications.[13-15] Both theoretical prediction and experimental results indicate that the (001) facets of anatase TiO_2 are much more reactive than other thermodynamically stable facets in photocatalytic oxidation.[16,17] Although great achievements have been made to design TiO_2 single-crystals with high percentage of exposed (001) facets reaching up to 90%,[18-23] their photocatalytic activity is still limited by the rapid electron-hole recombination.

Since the introduction of the use of heterojunctions in photocatalysis, the composite semiconductors have been widely designed to reduce the electron-hole recombination.[24,25] Most heterojunctions are constructed by random distribution of binary or ternary semiconductors. The charge transfer mainly occurs at the interface, which disfavors the photocatalytic reactions due to the diffusion limits of reactants toward the interface. Recently, Wang et al founded that the sharp edges of nanostructures could accelerate charge collection and separation as lightning rod effect, which supplied a driving force for directional electron transfer and also facilitated the reactions of electrons with reactants.[26] The composites between TiO_2 and carbon nanotubes (CNTs) exhibit enhanced activity due to the good electron conductivity of CNTs. However, the random combination between TiO_2 and the CNTs is unfavorable for the light harvesting, electron transfer, reactant diffusion and chemical reaction at active sites.[27] Besides, the weak interaction between the CNTs and TiO_2 usually causes poor durability of composite photocatalyst owing to the component leaching.[28]

Recently, we developed a microwave-hydrothermal synthesis of one-dimensional threaded nanocomposites by using Cu nanowires as microwave-antennas.[29] As good microwave absorber, the CNTs could also act as microwave-antennas, thereby inducing the nanomaterials self-assembly threaded onto the CNTs in the hierarchical structures. These nanocomposites can possess enhanced activity and stability in photocatalysis and energy storage due to the synergetic effects. Herein, we reported the synthesis of CNTs threaded anatase TiO_2 single-crystals with dominant (001) facets and enhanced activity in

[a] Education Ministry Key Lab of Resource Chemistry, Shanghai Key Laboratory of Rare Earth Functional Materials, International Joint Lab on Resource Chemistry SHNU-NUS-PU, Department of Chemistry, Shanghai Normal University, Shanghai 200234, China
[b] Department of Chemistry and Department of Physics, National University of Singapore, 3 Science Drive 3, 117543, Singapore.
E-mail: Dieqing Zhang, dqzhang@shnu.edu.cn; Wei Chen, phycw@nus.edu.sg; Hexing Li, Hexing-li@shnu.edu.cn.
† Electronic Supplementary Information (ESI) available: TG, FTIR, Raman, EPR and additional photocatalytic performance data. See DOI: 10.1039/x0xx00000x

photocatalytic NO oxidation under both UV and visible light irradiation.

Experimental section

Sample preparation

In a typical run of synthesis, 20 mg of the CNTs (untreated, diameter 60-100 nm) was well dispersed in an aqueous solution containing desired concentration of $TiCl_3$ by ultrasonication for 30 min. Then, 0.50 mL of the 1-methyl-imidazolium tetrafluoroborate ($Hmim[BF_4]$) was added. After being stirred for 10 min, the mixture was transferred into a 40 ml quartz vessel with a Teflon lid in a single chamber microwave synthesis system (Ultrawave, Milestone). It was then heated by microwave at a heating rate of 13 °C min^{-1} to 150 °C and kept at this temperature for 30 min under 35 bar of N_2 atmosphere. After being cooled down to room temperature, the solid products were collected and washed thoroughly with 0.10 M NaOH aqueous solution and DI water for three times. Finally, the products were calcined at 400 °C for 2 h, leading to the CNTs threaded TiO_2 nanocomposites (CNTs-TiO_2). We adjusted the concentration of the $TiCl_3$ in the initial solution of 0.050 M, 0.10 M, 0.20 M and 0.50 M (in order to keep the same amount of Ti source, the solution volumes were controlled as 48 mL, 24 mL, 12 mL and 4.8 mL, respectively). The as-prepared samples were labeled as CT1, CT2, CT3 and CT4, respectively. Calcination of CT4 in air at 700 °C for 4 h could completely remove the CNTs, leading to the pure TiO_2 and denoted as T4. T4-C refers to mechanical mixture of T4 and the CNTs with the same ratio as that in CT4. For comparison, C4 sample was also prepared by microwave heating the solution without the CNTs at 150 °C and keeping at this temperature for 30 min. Meanwhile, P4 was synthesized according to the procedure for preparing C4 by using $TiCl_4$ instead of $TiCl_3$. Sample CP4 was obtained in the same procedure as the CT4 by using $TiCl_4$ instead of $TiCl_3$. Finally, different CT4 samples were also synthesized by using CNTs pretreated in HNO_3 aqueous solution for different time (see Supplementary Information for experimental details).

Characterization

The crystal phase was determined by X-ray diffraction (XRD, Rigaku Dmax-3C Cu-Ka). Particle size and morphologies were observed on a transmission electron microscopy (TEM, JEOL-2010F, 200 kV) and a field scanning electron microscopy (FESEM, HITACHI, S-4800). Thermal gravimetric analysis (TGA) was performed by the PerkinElmer Pyris Diamond TG analyzer under air with a heating ramp of 5 °C min^{-1}. The photoluminescence spectra (PL) were examined on a Varian Cary-Eclipse 500 spectrometer. Surface electronic states were analyzed by X-ray photoelectron spectroscopy (XPS, Perkin-Elmer PHI 5000, Al-Kα). All the binding energy values were calibrated by using C1s = 284.6 eV as a reference. Raman spectra were recorded at room temperature using LabRam II confocal laser Raman system with a 632 nm laser as an excitation source. The electron paramagnetic resonance (EPR) spectra were recorded at 100 K using a Bruker EMX-8/2.7 EPR spectrometer. The UV-vis diffuse reflectance spectra (DRS) were obtained on a UV-vis spectrophotometer (UV-vis DRS, Shimadzu UV-2450). Fourier transform infrared (FT-IR) spectra were collected on a Nicolet Magna 550 spectrometer using the KBr method.

Photoelectrochemical measurement

The photocurrents and electrochemical impedance spectroscopy (EIS) measurements were carried out in a conventional three-electrode, single-compartment quartz cell on an electrochemical station (CHI 660D). Samples with an active area of *ca.* 4.0 cm^2 on an ITO glass were served as working electrode. The counter electrode and the reference electrode were platinum sheet and saturated calomel electrode (SCE), respectively. A bias voltage of 0.20 V was utilized for driven the photo-generated electrons transfer. A 6W 365 nm LED light located at 10 cm away from the photoelectrochemical cell was used as light source. A 0.50 M Na_2SO_4 aqueous solution was used as the electrolyte. The EIS tests were carried out at the bias of the open circuit voltage and recorded over a frequency ranged from 0.1 to 10^5 Hz with AC amplitude of 10 mV.

Photocatalytic NO Oxidation

The photocatalytic NO oxidation in gas phase was carried out at ambient temperature in a continuous flow reactor with volume of 10.8 L (42 × 26 × 27 cm). For the UV light driven photocatalysis, eight 6w 365 nm UV lamps located vertically above the reactor were used as light source. Two 150 W of halogen lamps were used as the solar light source. The visible light photocatalytic reaction was carried out under two 150 W of halogen lamps irradiation equipped with a UV cut filter to cut off light with the wavelength < 400 nm. In each run of experiments, an ultrapure air gas flow containing 500 ppb NO was allowed to pass through a photocatalyst containing 0.20 g TiO_2 at the rate of 4.0 L/min. After reaching adsorption-desorption equilibrium on the photocatalyst, the lamps were turned on to start the photocatalytic reaction. The concentration of NO was continuously measured by the chemiluminescence NO analyzer (Thermo Environmental Instruments Inc. Model 42i). The NO removal ratio (%) was calculated based on the following equation: NO removal rate (%) = $(C_0 - C)/C_0 \times 100\%$, where C_0 and C refer to the NO concentration determined before and after the reaction.

Results and discussion

Structural characteristics

As shown in Fig. 1, both the FESEM and the TEM images revealed that the as-prepared CNTs-TiO_2 composites comprised CNTs threaded TiO_2 decahedral nanocrystals with average rectangular side length of ca. 700-800 nm and thickness of ca. 400 nm. The HRTEM showed the perpendicular lattice spacing of ca. 0.189 nm, corresponding to the (020) and (220) planes of anatase TiO_2 crystals. The attached SAED pattern confirmed that the anatase TiO_2 single crystal grew along the [00-4] zone axis with (200) and (020) planes, leading to the exposed (001) facets, which was consistent with the HRTEM image. Meanwhile, it also displayed three concentric diffraction circles corresponding to the high degree of graphitization of the CNTs. From CT1 to CT4, with the increase of the TiO_2 content, the length of the TiO_2 decahedron increased slightly while the thickness decreased, showing the enhanced percentage of

exposed (001) facets in anatase TiO_2 decahedrons threaded by CNTs.

The XRD patterns in Fig. 2a further demonstrated the single-crystalline structure of anatase TiO_2 in all CNTs-TiO_2 composites prepared by microwave heating, corresponding to the diffractions of (101), (103), (004), (112), (200), (105), (211), (204), (116), (220) and (215) at 2θ around 25.3, 36.9, 37.8, 38.6, 48.0, 53.9, 55.1, 62.7, 68.8, 70.3 and 75.0° (JC-PDF 21-1272). A small peak around 2θ of 26.4° could be assigned to CNTs. The appearance of diffraction peak at 2θ around 37.8° indicated the oriented crystal-growth, leading to the exposed (001) facets. According to the intensities of (101), (200), and (004) diffractions, the percentage of exposed (001) facets could be calculated by using the crystal model and the Scherrer equation (details shown in the Supplementary Information，Fig. S1).[30] From CT1 to CT4 with the increasing of TiO_2 content, the percentage of exposed (001) increased in the order of 62%, 68%, 76% and 84%, which was in good accordance with the above FESEM characterization. The T4 obtained by calcination of CT4 in air at 700 °C for 4 h displayed almost the same XRD pattern as the CT4. However, the diffraction peak indicated the disappearance of CNTs, suggesting the complete removal of CNTs. Comparing to T4, there was no significant position shift of the principal diffraction peaks in CT4, indicating no CNTs incorporated into the TiO_2 lattice.

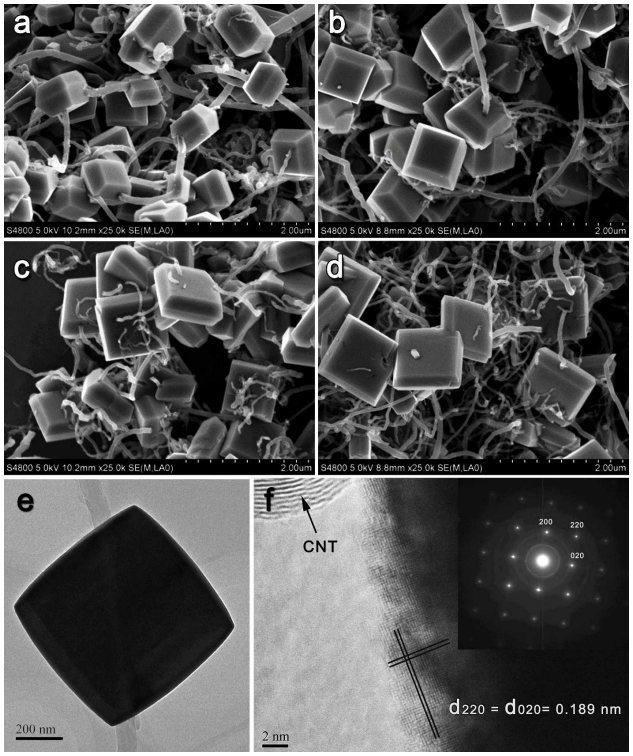

Fig. 1 FESEM images of (a-d) CT1-CT4, TEM (e) and HRTEM (f) images of CT4, together with the SAED images of CT4 (inset).

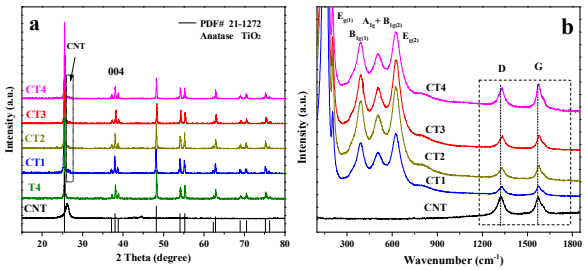

Fig. 2 (a) XRD patterns of different samples and (b) Raman spectra of pure CNTs and CNTs-TiO2 composites.

Raman spectra (Fig. 2b) of all the CNTs-TiO_2 composites showed two well-resolved bands at 1325 and 1574 cm^{-1}, corresponding to the D-band and G-band related to the disordered sp^2 carbon and the well graphitized carbon in the CNTs.[31] In comparison with pure CNTs, those peaks slightly broadened and blue-shifted due to the strong interaction between CNTs and TiO_2.[32,33] Meanwhile, the CT1 to CT4 samples displayed the similar intensities of D-band and G-band, implying the same CNTs amount, which could be further confirmed by the similar weight loss in TG curves (Fig. S2). In comparison with pure CNTs, the CNTs-TiO_2 composites displayed additional bands with very high intensities at 146.0, 389.4, 506.5 and 626.2 cm^{-1}, corresponding to the typical $E_{g(1)}$, $B_{1g(1)}$, A_{1g}+$B_{1g(2)}$ and $E_{g(2)}$ vibration modes of anatase TiO_2.[34-36]

As shown in Fig. 3(a), after curve fitting in the C 1s core level XPS spectrum, the CT4 displayed four well resolved peaks around binding energies of 284.6, 285.4, 286.9 and 288.8 eV, respectively. Those peaks could be assigned to the sp^2 hybridized carbon (C-C), the defect of sp^2 carbon, oxygen-containing species of the hydroxyl group (C-O) and the carboxyl group (O-C=O),[37] which could be confirmed by FT-IR spectra (Fig. S3). Meanwhile, the CT4 showed a strong peak located at the binding energy of 458.3 eV in the Ti $2p_{3/2}$ core level spectrum (Fig. 3b). In comparison with that of the CP4 obtained by using $TiCl_4$ instead of $TiCl_3$ as the Ti source, the $Ti2p_{3/2}$ of CT4 shifted towards lower binding energy by 0.2 eV, indicating the presence of Ti^{3+}.[38-40] The EPR spectrum (Fig. S4) further confirmed the presence of Ti^{3+}, corresponding to the appearance of a strong signal located at the g = 1.96.

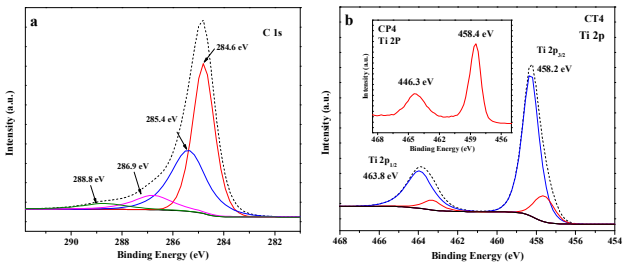

Fig. 3 (a) C1s fine scan XPS spectra of sample and (b) Ti 2p fine scan XPS spectra of CT4 and CP4 (inset).

The Uv-vis DRS spectra in Fig. 4a revealed that CT1, CT2, CT3 and CT4 exhibited the similar light absorbance due to the similar structure and composition. Both the CT4 and C4 obtained by using $TiCl_3$ as the Ti source with and without adding the CNTs displayed strong absorbance in visible region, corresponding to a lower band gap (E_g) of 3.0 eV, which is obviously due to the Ti^{3+} self-doping effect. The P4 sample prepared by using $TiCl_4$ instead of $TiCl_3$ displayed no significant spectral response in visible region, showing a larger E_g of pure anatase TiO_2 (3.2 eV).[41,42] CT4 exhibited much higher absorption capacity in the visible light region than C4, corresponding to the color change from white to grey. The FESEM image (Fig. S5) revealed that C4 displayed severe aggregation of TiO_2 nanocrystals in comparison with CT4 (Fig. 1). Thus, the higher light absorption of CT4 than that of C4 could be mainly attributed to the enhanced light harvesting due to the well assembly of TiO_2 nanocrystals along the CNTs, arising from the enhanced multiple light reflections.[43] Fig. 4b indicated that the photocurrent intensity increased in the order from CT1 to CT4. Taking into account that they exhibited similar light absorbance, this could be mainly ascribed to the decreasing electron-hole recombination rate. This could be confirmed by PL spectra in Fig. 4c, corresponding to slight decrease in intensity of the excitation peak around 560 nm.[38] Although the crystal size and BET surface area remained almost unchanged (Table S1), the thickness of TiO_2 decahedrons decreased from CT1 to CT4, together with higher density of TiO_2 nanocrystals threaded by CNTs (Fig. 1). Thus, photo-induced electrons could be easily separated from TiO_2 to CNTs *via* their heterojunctions and rapidly transferred through the CNTs with good electron conductivity, leading to the reduced electron-hole recombination probability. T4-C showed the decrease in photocurrent intensity comparing to CT4 since the mechanical mixture of TiO_2 and CNTs displayed much lower number of heterojunctions, leading to the increased difficulty in electron transfer, consistent with the enlarged semicircles of the EIS spectra in Fig. 4d. In addition, T4 displayed even lower photocurrent response than T4-C because of the absence CNTs for transferring photo-induced electrons,[44] leading to an abrupt increase of impedance comparing to CT4.[45,46] Thus, the electron-hole recombination rate increased, corresponding to the enhanced intensity of PL peak around 560 nm in Fig. 4c. As expected, C4 displayed the lowest photocurrent response. On one hand, it showed very poor light harvesting due to the aggregation of TiO_2 nanocrystals; on the other hand, it showed high electron-hole recombination rate in absence of the CNTs, corresponding to the strongest intensity of PL peak in Fig. 4c.

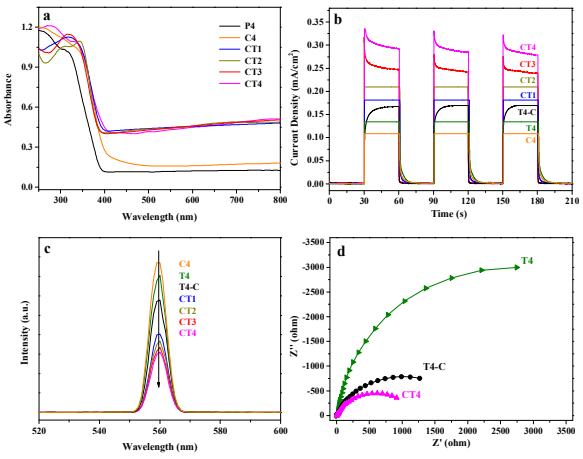

Fig. 4 (a) The UV-vis DRS spectra, (b) transient photocurrent responses, (c) PL spectra and (d) EIS spectra of different photocatalysts.

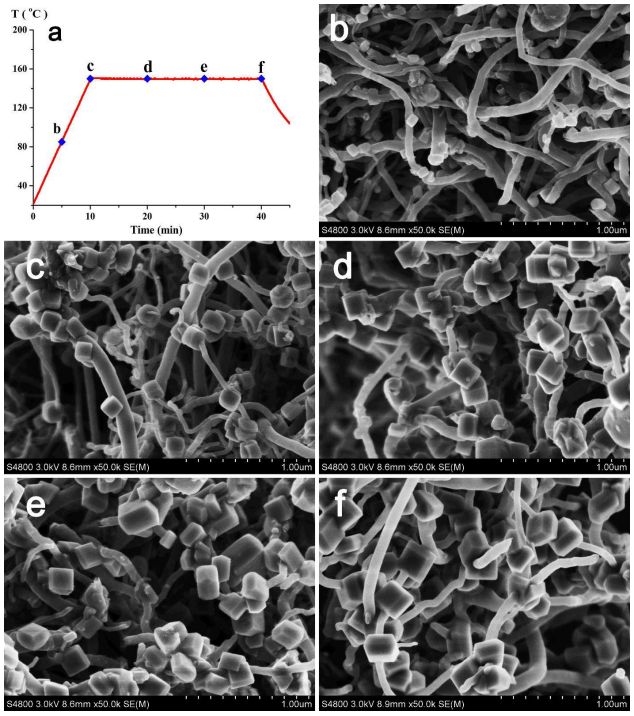

Fig. 5 Reaction progress (a) and the FESEM images CT4 obtained at microwave-heating for 5 min to 85 °C (b) and for 10 min to 150 °C, followed by keeping at this temperature for (c) 0, (d) 10, (e) 20, and (f) 30 min.

Growth mechanism

Fig. 5 shows the reaction progress for synthesizing CT4 samples at different microwave heating time and the corresponding solution temperature (a), together with their FESEM images (b-f). When the microwave heating temperature was lower than 85 °C, no reaction occurred. As shown in Fig. 5b, when the reaction mixture was heated for 5 min to 85 °C by microwave irradiation, anatase TiO_2 single-crystals (see the XRD pattern in Fig. S6) were found on the CNTs surface. Increase of microwave heating time to 10 min reaching 150 °C resulted in the crystal growth (Fig. 5c). Fig. 5c to 5f clearly demonstrated that, by keeping the temperature at 150 °C, increase of the microwave-ionothermal treatment time from 0 to 30 min further promoted TiO_2 crystal-growth into decahedrons with exposed (001) facets, together with the rapid increasing density of TiO_2 nanocrystals threaded by the CNTs.

The above results demonstrated the important roles played by both the presence of CNTs and the microwave heating. The CNTs acted as microwave-antennas to strongly absorb microwaves, followed by converting microwave energy into heat to generate surface "super hot" dots. Because of the high temperature comparing to the bulk

solution, those "super hot" dots induced the adsorption of Ti^{3+} and the subsequent hydrolysis/oxidation of Ti^{3+} into TiO_2 single crystals, which could grow and assemble along the CNTs. Microwave heating to 85 °C was proved to be the critical temperature to initiate the growth of the CNTs threaded TiO_2 nanocrystals. No TiO_2 nanocrystal was observed at this temperature either in the absence of CNTs or by using traditional autoclave heating instead of microwave heating. This could further confirm the presence of "super hot" dots on CNTs generated by microwave rather than traditional heating. Although the temperature was very low in the bulk solution, the temperature of "super hot" dots was high enough to initiate the hydrolysis and oxidation of adsorbed Ti^{3+} to form TiO_2 single crystals. This can ensure that all TiO_2 nanocrystals were anchored on the CNTs. With the increase of microwave heating temperature from 85 °C to 150 °C, the TiO_2 could grow into large-sized single crystals threaded by the CNTs. Keeping the microwave temperature at 150 °C, the TiO_2 nanocrystal would continuously grow with the transformation from nanocubes to nanodecahedrons. Meanwhile, the density of the TiO_2 nanocrystals threaded on the CNTs increased rapidly since more and more "super hot" dots could be generated on the CNTs surface. The single-crystalline TiO_2 could also be synthesized in the absence of CNTs under the same conditions. However, the FESEM image (Fig. S5) displayed the large-sized TiO_2 decahedrons with severe agglomeration. These results further confirmed that the microwave heating ensured the formation of TiO_2 nanocrystals onto the CNTs rather than in the solution due to the "super hot" dots with high temperature on the CTNs surface, which could greatly reduce the aggregation of TiO_2 nanocrystals.

To further examine the ability of CNTs for absorbing microwaves, the CNTs (3.0 g) were treated in 90 mL 65 wt% HNO_3 aqueous solution at 90 °C for 30, 60 and 120 min, respectively. The FT-IR spectra (Fig. S2) revealed that the amount of surface carboxyl and hydroxyl groups increased, corresponding to the increasing intensity of the absorbance bands at 1640 and 3460 cm^{-1}. This could be further confirmed by Raman spectra (Fig. S7), where the decreased I_D/I_G was due to the increased amount of oxygen groups on CNTs surface. As well known, the microwave absorption ability of CNTs increased with the increase of surface carboxyl and hydroxyl groups. The FESEM images (Fig. S8) demonstrated that the density of TiO_2 nanocrystals on the CNTs increased with the increased amount of the surface carboxyl and hydroxyl groups compared with the CT3 samples prepared by using untreated CNTs. However, no significant change in either the TiO_2 shape or the TiO_2 particle size was found, indicating that the HNO_3-treatment mainly increased the number rather than the temperature of "super hot" dots on CNTs surface.

It is worth mentioning that the Hmim[BF_4] ionic liquid played an crucial role in the *in-situ* synthesis of CNTs threaded TiO_2 nanocrystals with exposed (001) facets. As shown in Fig. 6a, b and c, the FESEM images and XRD patterns demonstrated that the CT4 synthesized in the presence of Hmim[BF_4] displayed anatase TiO_2 decahedrons threaded by CNTs. However, the CT4 synthesized in the absence of ionic liquid displayed rutile TiO_2 nanorods threaded by CNTs. Meanwhile, it was also found that the $TiCl_3$ aqueous solution without adding ionic liquid showed violet color while the $TiCl_3$ aqueous solution with 1.5 wt% ionic liquid displayed brown-green color (Fig. 6d), indicating the coordination of Ti^{3+} with $[BF_4]^-$. Thus, the formation of rutile and anatase TiO_2 could be briefly illustrated in Fig. 6e. In the absence of Hmim[BF_4], the Ti^{3+} could easily hydrolyze into $TiOH^{2+}$ and subsequently oxidized into TiO_2 crystal-cells in the form of TiO_6 octahedrons (see the following Equation 1 to 3). Those TiO_6 octahedrons linked linearly by sharing the pair of the opposite edges, corresponding to the typical arrangement for single-crystalline rutile TiO_2 nanorods.[47,48] However, in the presence of Hmim[BF_4], the Ti^{3+} would firstly coordinate with $[BF_4]^-$, followed by oxidizing into TiO_2 crystal cells in the form TiO_6 octahedrons (see the following Equation 4 to 5). Since the presence of $[BF_4]^-$ could inhibit the growth of edges-shared TiO_6 octahedron,[49] the TiO_6 octahedrons could be linked mainly along [221] direction to form a two-dimensional "Z-chains", leading to the formation of the single-crystalline anatase TiO_2. More importantly, the Hmim[BF_4] ionic liquid provided a plenty of fluorine sources due to the presence of $[BF_4]^-$.[23] Normally, the TiO_2 crystals would grow along all three-dimensions to form octahedron with exposed (101) facets. However, the F^- or $[BF_4]^-$ ions could be easily adsorbed onto the (001) facets, which could efficiently inhibit the TiO_2 crystal-growth along vertical axis, leading to the formation of decahedrons with exposed (001) facets.[30]

$$[Ti(H_2O)_6]^{3+} + H_2O \rightarrow [TiOH(H_2O)_5]^{2+} + H_3O^+ \quad (1)$$

$$[TiOH(H_2O)_5]^{2+} + O_2 \rightarrow [TiOH(H_2O)_5]^{3+} \quad (2)$$

$$[TiOH(H_2O)_5]^{3+} + H_2O \rightarrow TiO_2\ (\text{Rutile}) \quad (3)$$

$$[Ti(H_2O)_6]^{3+} + BF_4^- \rightarrow [Ti(BF_4)_m(H_2O)_{6-m}]^{(3-m)+} + H_3O^+ \quad (4)$$

$$[Ti(BF_4)_m(H_2O)_{6-m}]^{(3-m)+} + H_2O \rightarrow [Ti(OH)_4(BF_4)_m(H_2O)_{6-m}]^0 \rightarrow TiO_2\ (\text{Anatase}) \quad (5)$$

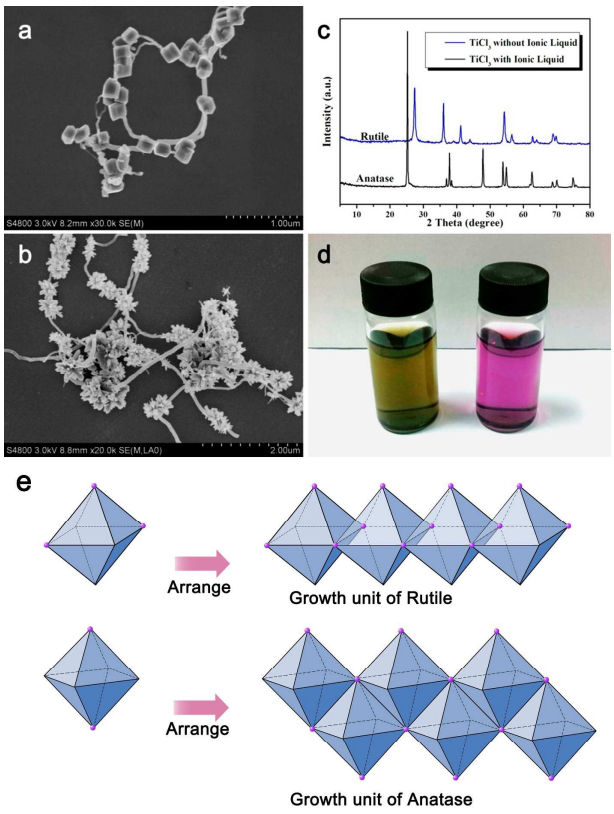

Fig. 6 FESEM images of CT4 prepared with (a) and without Hmim[BF_4], together with the XRD patterns (c) and (d) color comparison of 10 mL 1.5 wt% $TiCl_3$ solution with (left) and without Hmim[BF_4] (right). (e) A possible linkage of TiO_6 octahedrons into anatase and rutile TiO_2 nuclei.

Photocatalytic performance

Gas-phase photocatalytic nitric oxide (NO) oxidation was used as a probe to evaluate the performance of different photocatalysts. Since no significant decrease of NO content was detected in the absence of either photocatalyst or light irradiation and no significant activity of pure CNTs was observed, the main active site can be ascribed to TiO_2 in this photocatalytic system. Fig. 7a summarized the activities of different samples for photocatalytic NO oxidation under 365 nm UV light irradiation. Firstly, the activity increased from CT1 to CT4. Because of the similar CNTs content, crystallite size and BET surface area (see Fig. S2 and Table S1), together with only slight decrease in electron-hole recombination rate (Fig. 4c), we therefore concluded that the increased activity was mainly due to the increase of exposed (001) facets of anatase TiO_2 from 62% to 84%. Meanwhile, the CT4 exhibited much higher activity than T4 obtained by calcination of CT4 to remove the CNTs. This could be mainly attributed to the low electron-hole recombination rate of CT4 since the calcinations had no significant influence on either the BET surface area or the percentage of exposed (001) facets. T4-C obtained by mechanically mixing pure TiO_2 (T4) with CNTs showed slightly higher activity than T4 since the CNTs facilitated electron transfer and hence reduced their recombination with holes. However, T4-C still exhibited much lower activity than CT4 because of the weak interaction of TiO_2 with CNTs via such mechanical mixing treatment. The well assembly of TiO_2 along the CNTs in CT4 could promote the electron transfer and thus efficiently inhibit the electron-hole recombination. C4 exhibited the lowest activity due to the poor light harvesting, the strong reactant diffusion limit, and the high electron-hole recombination rate, which could arise from the self-aggregation of TiO_2 nanocrystals and the absence of the CNTs for efficient electron transfer. Besides the high activity, CT4 also exhibited strong durability and stability.

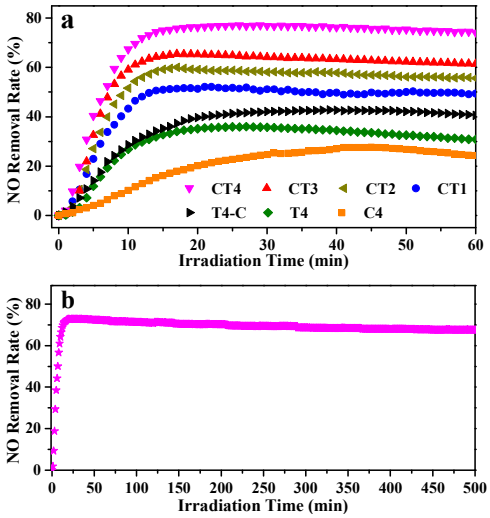

Fig. 7 (a) Reaction profiles of UV lights (365 nm) driven photocatalytic NO oxidation on different photocatalysts and (b) Recycling test of the CT4.

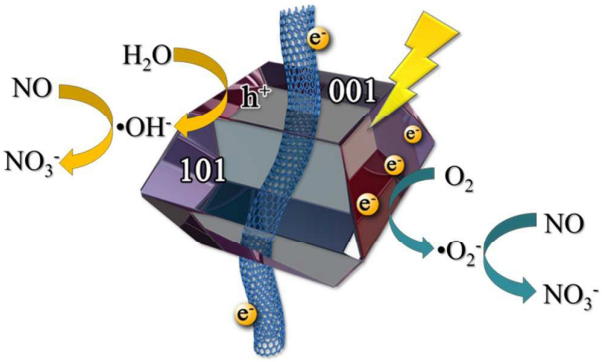

Fig. 8 Proposed photocatalytic mechanism for NO oxidation.

As shown in Fig. 7b, it could be used continuously for more than 500 min without significant deactivation. The high stability of CT4 could be attributed to the strong interaction between TiO_2 and the CNTs, which could efficiently inhibit both the aggregation and the leaching of TiO_2 nanocrystals during photocatalytic reaction. We also carried out controlled experiments to optimize the catalysts by adjusting the CNTs amount and surface properties of the CNTs. Fig. S9 demonstrated that the CT4 prepared by using 20 mg CNTs in the initial solution exhibited higher photocatalytic activity than those prepared by using either lower amount (0, 5.0, 10 mg) or higher amount (40 mg) of CNTs. The photocatalytic activity first increased with increasing CNTs amount due to the well assembly of TiO_2 nanocrystals onto the CNTs favoring light harvesting and the enhanced electron transfer with the increasing CNTs amount, which facilitated their separation from holes. However, very high CNTs amount was harmful for the photocatalytic activity, which is due to the light shielding effect by the extra CNTs. It was also found that CT3 photocatalysts prepared by using untreated CNTs exhibited higher activity than those by using HNO_3-treated CNTs, and the activity decreased with the increase of HNO_3-treatment time (see Fig. S10). On one hand, the long HNO_3-treatment of CNTs resulted in the enhanced density of TiO_2 nanocrystals on CNTs, which was unfavorable for either the light harvesting or reactant diffusion and adsorption. On the other hand, the long HNO_3-treatment of CNTs resulted in rapid electron-hole recombination, consistent with the enhanced intensity of PL peak around 560 nm (Fig. S11a).[50, 51] The long HNO_3-treatment induced more defects on the CNTs surface (see Raman spectra in Fig. S7), which disfavored the electron transfer and was consistent with the enhanced impedance in EIS spectra (Fig. S11b). Meanwhile, the long HNO_3-treatment also increased the amount of electron-rich oxygen groups on CNTs surface (see Fig. S2), which could reversely transfer electrons from CNTs to TiO_2, thereby increasing electron-hole recombination rate.[52]

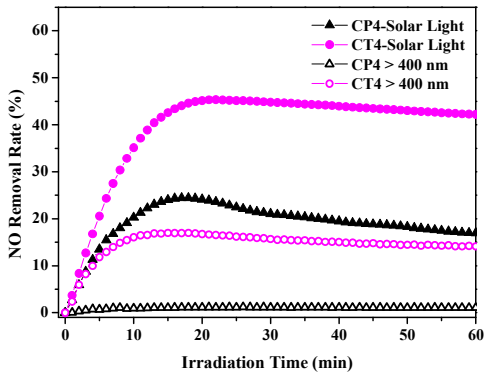

Fig. 9 Photocatalytic performances of CT4 and CP4 in photocatalytic NO oxidation irradiated with solar lights and visible lights (λ >400 nm), respectively.

In this photocatalytic reaction, NO was removed mainly by photocatalytic oxidation in which the main products were determined to be NO_2 and NO_3^-. The roles played by TiO_2 and CNTs were illustrated in Fig. 8. Firstly, TiO_2 was activated under UV light irradiation to generate electrons and holes. Then, the electrons transferred from (001) to (101) facets of TiO_2 through the CNTs electron conductor and left holes on the (001) facets. Those electrons and holes further reacted with O_2 and H_2O to generate superoxide radicals ($\cdot O_2^-$) and hydroxyl radicals ($\cdot OH$),[53] respectively, which could directly oxidize NO into NO_2 and NO_3^- etc.[8,54] Both experimental investigation and theoretical prediction demonstrated that the (001) facet was more active than the other facets like (101) in photocatalytic oxidation due to the high surface energy, which favored the dissociation of adsorbed molecules.[16,17,55]. Therefore, for the CNT-TiO_2 composites, the high efficiency of photocatalytic NO oxidation was mainly dependent on (1) efficient light harvesting and reactant adsorption properties, (2) fast electron transfer by the CNTs and low electron-hole recombination rate, and (3) high percentage of exposed active (001) facets of anatase TiO_2.

Furthermore, as shown in Figure 9, CT4 also exhibited the NO removal ratios of 46.7% under solar light irradiation and 17.4% under visible light (λ >400 nm), showing good potential for practical applications. On contrast, CP4 obtained in the same procedure as the CT4 by using $TiCl_4$ instead of $TiCl_3$ exhibited negligible activity under visible light (λ >400 nm) and very poor activity under solar light due to the larger band gap of pure anatase TiO_2 (3.2 eV). CT4 displayed visible light induced photocatalytic activity mainly due to the Ti^{3+}-doped TiO_2 (see Figure 4a).[41, 42]

Conclusions

In conclusion, CNTs threaded TiO_2 single-crystals with exposed (001) facets were fabricated by a one-step microwave-ionothermal strategy. The phase transformation of TiO_2 from rutile to anatase induced by $[BF_4]^-$ groups was reported for the first time. The prepared CT4 sample with 84 % percentage of (001) facets showed the highest photocatalytic NO removal ratio up to 76.8 % under UV irradiation and also shows photocatalytic activities under irradiation with either solar lights or visible lights due to the self-doped Ti^{3+}. In addition, the CNTs possess microwave irradiation induced surface "super hot" dots, thereby accelerating the direct growth of TiO_2 crystals and avoiding the aggregation of TiO_2 during the synthesis. Meanwhile, by manipulating the surface chemistry of CNTs, reliable catalysts can be rationally designed. For the photocatalytic reaction, CNTs served as a direct-charge transport superhighway among threaded TiO_2 single crystal with tunable percentage of exposed (001) active facet, which synergistically promoted the solar-driven NO removal. This study promises a novel and efficient way for catalyst design for their potential applications in environmental and energy research fields.

Acknowledgements

This work was supported by the NSFC (21477079, 21207090, 21261140333 and 21237003), Shanghai Government (13YZ054, 14ZR1430900, 15QA1403300), PCSIRT (IRT1269), the doctoral program of higher education (20123127120009) and SHNU (S30406), and Singapore MOE Tier II grant of R143-000-542-112.

Notes and references

1 R. Asahi, T. Morikawa, T. Ohwaki, K. Aoki and Y. Taga, *Science (New York, N.Y.)*, 2001, **293**, 269-271.
2 X. Chen and S. S. Mao, *Chem. Rev.*, 2007, **107**, 2891-2959.
3 A. Kudo and Y. Miseki, *Chem. Soc. Rev.*, 2009, **38**, 253-278.
4 I. Nakamura, N. Negishi, S. Kutsuna, T. Ihara, S. Sugihara and K. Takeuchi, *J. Mol. Catal. A-chem.*, 2000, **161**, 205-212.
5 Z. Ai, W. Ho and S. Lee, *J. Phys. Chem. C*, 2011, **115**, 25330-25337.
6 Z. Ai, W. Ho, S. Lee and L. Zhang, *Environ. Sci. Technol.*, 2009, **43**, 4143-4150.
7 T. Sano, S. Tsutsui, K. Koike, T. Hirakawa, Y. Teramoto, N. Negishi and K. Takeuchi, *J. Mater. Chem. A*, 2013, **1**, 6489-6496.
8 D. Zhang, M. Wen, S. Zhang, P. Liu, W. Zhu, G. Li and H. Li, *Appl. Catal. B-environ*, 2014, **147**, 610-616.
9 Y. Huang, W. Ho, Z. Ai, X. Song, L. Zhang and S. Lee, *Appl. Catal. B-environ*, 2009, **89**, 398-405.
10 X. Lang, W. Ma, C. Chen, H. Ji and J. Zhao, *Accounts. Chem. Res.*, 2014, **47**, 355-363.
11 P. V. Kamat, *J. Phys. Chem. C*, 2007, **111**, 2834-2860.
12 X. Chen, S. Shen, L. Guo and S. S. Mao, *Chem. Rev.*, 2010, **110**, 6503-6570.
13 E. J. Crossland, N. Noel, V. Sivaram, T. Leijtens, J. A. Alexander-Webber and H. J. Snaith, *Nature*, 2013, **495**, 215-219.
14 G. Liu, C. Sun, H. G. Yang, S. C. Smith, L. Wang, G. Q. Lu and H.-M. Cheng, *Chem. Commun.*, 2010, **46**, 755-757.
15 N. Wu, J. Wang, D. N. Tafen, H. Wang, J.-G. Zheng, J. P. Lewis, X. Liu, S. S. Leonard and A. Manivannan, *J. Am. Chem. Soc.*, 2010, **132**, 6679-6685.

16 X.-Q. Gong and A. Selloni, *J. Phys. Chem. B*, 2005, **109**, 19560-19562.
17 M. Kamei and T. Mitsuhashi, *Surf. Sci.*, 2000, **463**, L609-L612.
18 W. Yang, J. Li, Y. Wang, F. Zhu, W. Shi, F. Wan and D. Xu, *Chem. Commun.*, 2011, **47**, 1809-1811.
19 L. Ye, J. Mao, J. Liu, Z. Jiang, T. Peng and L. Zan, *J. Mater. Chem. A*, 2013, **1**, 10532-10537.
20 X. Han, Q. Kuang, M. Jin, Z. Xie and L. Zheng, *J. Am. Chem. Soc.*, 2009, **131**, 3152-+.
21 H. G. Yang, G. Liu, S. Z. Qiao, C. H. Sun, Y. G. Jin, S. C. Smith, J. Zou, H. M. Cheng and G. Q. Lu, *J. Am. Chem. Soc.*, 2009, **131**, 4078-4083.
22 H. G. Yang, C. H. Sun, S. Z. Qiao, J. Zou, G. Liu, S. C. Smith, H. M. Cheng and G. Q. Lu, *Nature*, 2008, **453**, 638-634.
23 D. Zhang, G. Li, X. Yang and J. C. Yu, *Chem. Commun.*, 2009, 4381-4383
24 J. Yu, T. Ma and S. Liu, *Phys. Chem. Chem. Phys.*, 2011, **13**, 3491-3501.
25 Q. Xiang, J. Yu and M. Jaroniec, *Chem. Soc. Rev.*, 2012, **41**, 782-796.
26 L. He, C. Wang, X. Yao, R. Ma, H. Wang, P. Chen and K. Zhang, *Carbon*, 2014, **75**, 345-352.
27 Y. Yao, G. Li, S. Ciston, R. M. Lueptow and K. A. Gray, *Environ. Sci. Technol.*, 2008, **42**, 4952-4957.
28 W. Guo, C. Xu, X. Wang, S. Wang, C. Pan, C. Lin and Z. L. Wang, *J. Am. Chem. Soc.*, 2012, **134**, 4437-4441.
29 S. Xiao, P. Liu, W. Zhu, G. Li, D. Zhang and H. Li, *Nano Lett.*, 2015, **15**, 4853-4858.
30 J. Zhu, S. Wang, Z. Bian, S. Xie, C. Cai, J. Wang, H. Yang and H. Li, *CrystEngComm*, 2010, **12**, 2219-2224.
31 H. Hiura, T. Ebbesen, K. Tanigaki and H. Takahashi, *Chem. Phys. Lett.*, 1993, **202**, 509-512.
32 C. Chen, W. Cai, M. Long, B. Zhou, Y. Wu, D. Wu and Y. Feng, *ACS Nano*, 2010, **4**, 6425-6432.
33 L.-W. Zhang, H.-B. Fu and Y.-F. Zhu, *Adv. Funct. Mater*, 2008, **18**, 2180-2189.
34 T. Ohsaka, F. Izumi and Y. Fujiki, *J. Raman Spectrosc.*, 1978, **7**, 321-324.
35 S. Liu, J. Yu and S. Mann, *J. Phys. Chem. C*, 2009, **113**, 10712-10717.
36 J. Zhang, M. Li, Z. Feng, J. Chen and C. Li, *J. Phys. Chem. B*, 2006, **110**, 927-935.
37 J. Li, S. Tang, L. Lu and H. C. Zeng, *J. Am. Chem. Soc.*, 2007, **129**, 9401-9409.
38 X. Yang, C. Cao, L. Erickson, K. Hohn, R. Maghirang and K. Klabunde, *J. Catal.*, 2008, **260**, 128-133.
39 S. Hoang, S. P. Berglund, N. T. Hahn, A. J. Bard and C. B. Mullins, *J. Am. Chem. Soc.*, 2012, **134**, 3659-3662.
40 X. Liu, S. Gao, H. Xu, Z. Lou, W. Wang, B. Huang and Y. Dai, *Nanoscale*, 2013, **5**, 1870-1875.
41 F. Zuo, L. Wang, T. Wu, Z. Zhang, D. Borchardt and P. Feng, *J. Am. Chem. Soc.*, 2010, **132**, 11856-11857.
42 M. Xing, W. Fang, M. Nasir, Y. Ma, J. Zhang and M. Anpo, *J. Catal.*, 2013, **297**, 236-243.
43 H. Li, Z. Bian, J. Zhu, D. Zhang, G. Li, Y. Huo, H. Li and Y. Lu, *J. Am. Chem. Soc.*, 2007, **129**, 8406-+.
44 J. Kim, D. Monllor-Satoca and W. Choi, *Energy Environ. Sci.*, 2012, **5**, 7647-7656.
45 X. Bai, L. Wang and Y. Zhu, *ACS Catalysis*, 2012, **2**, 2769-2778.
46 46. R. Fang, G. Zhou, S. Pei, F. Li and H.-M. Cheng, *Chem. Commun.*, 2015, **51**, 3667-3670.
47 E. Hosono, S. Fujihara, K. Kakiuchi and H. Imai, *J. Am. Chem. Soc.*, 2004, **126**, 7790-7791.
48 A. Kumar, A. R. Madaria and C. Zhou, *J. Phys. Chem. C*, 2010, **114**, 7787-7792.
49 J. Yu, S. Liu and H. Yu, *J. Catal.*, 2007, **249**, 59-66.
50 Y. Huo, Z. Bian, X. Zhang, Y. Jin, J. Zhu and H. Li, *J. Phys. Chem. C*, 2008, **112**, 6546-6550.
51 Z. Bian, J. Zhu, F. Cao, Y. Lu and H. Li, *Chem. Commun.*, 2009, 3789-3791.
52 W. Chen, J. Ji, X. Duan, G. Qian, P. Li, X. Zhou, D. Chen and W. Yuan, *Chem. Commun.*, 2014, **50**, 2142-2144.
53 T. Tachikawa, S. Yamashita and T. Majima, *J. Am. Chem. Soc.*, 2011, **133**, 7197-7204.
54 G. Li, D. Zhang and J. C. Yu, *Chem. Mater.*, 2008, **20**, 3983-3992.
55 A. Vittadini, A. Selloni, F. Rotzinger and M. Grätzel, *Phys. Rev. Lett.*, 1998, **81**, 2954.

Nanoscale

ARTICLE

TOC graph

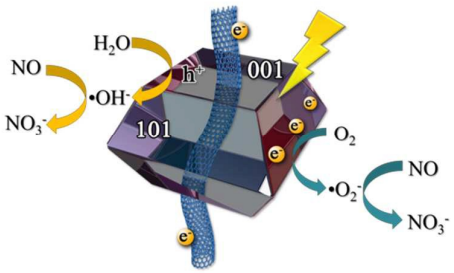

CNTs-threaded (001) exposed TiO_2 provides high percentage of active facets and direct electron highway to largely enhance solar NO oxidation.